Springer

Available online at https://link.springer.com/journal/42241
http://www.jhydrodynamics.com
Journal of Hydrodynamics, 2022, 34(5): 904-916
https://doi.org/10.1007/s42241-022-0069-5

Aeration performances and air-water mass transfer on steep stepped weirs with horizontal and inclined steps

Yvan Arosquipa Nina[1], Rui Shi[1], Davide Wüthrich[1, 2], Hubert Chanson[1*]
1. *The University of Queensland, School of Civil Engineering, Brisbane, Australia*
2. *Department of Hydraulic Engineering, Delft University of Technology, Delft, The Netherlands*

(Received September 20, 2021, Revised July 11, 2022, Accepted August 5, 2022, Published online November 3, 2022)

Abstract: At hydraulic structures, some strong interactions may develop between fast flowing waters and the air adjacent to the water in motion that enhance the air-water transfer of atmospheric and volatile gases in the flow. In turn, in-stream structures may contribute to the aeration and re-oxygenation during overflow. The present study aims to characterize the aeration performance of a steep stepped weir, based upon a detailed physical investigation of air-water interfacial properties across a relatively wide range of discharges. The data showed a strong fragmentation of the air-water flows, a very broad range of entrained bubbles and drops, and a large amount of particle clustering. The results implied a monotonic increase in re-aeration with increasing rate of energy dissipation, while the largest aeration efficiency was observed on the horizontal step weir chute, with the smallest on the 1V:2.33H inclined downward steps. Altogether, the study showed that a steep stepped chute can make a sizeable contribution to the re-oxygenation of the waters, although the downward inclined steps reduce the re-aeration performances.

Key words: Stepped weirs, aeration, re-oxygenation, physical modeling, flow fragmentation

Introduction

At hydraulic structures, some strong interactions may develop between fast flowing waters and the air adjacent to the water in motion. These interactions may or not be beneficial. The effects of air-water interactions include some bulking of the nappe, with adverse impact in tunnel spillways, bottom outlets and dropshafts[1-2], some drag reduction along steep chutes[3-4], the prevention of cavitation damage[5] and the air-water transfer of atmospheric gases[6]. Pertinent reviews on the topic include the textbooks by Rao and Kobus[1], Wood[5] and Chanson[7].

In self-aerated chute flows, the air-water transfer of atmospheric and volatile gases, e.g., oxygen, nitrogen, carbon dioxide, volatile organic compounds, is enhanced by the very-strong turbulence and large air-water interfacial area. In turn, the downstream water quality is modified. While the mass transfer is a relatively slow process, e.g. compared with interfacial processes such as bubble breakup and coalescence, the effects may become significant in highly-aerated flows and long channels. For example, saturation and even supersaturation of dissolved oxygen and nitrogen have been reported downstream of spillways, storm waterways and cascades[8]. Aeration enhancement by macro-roughness is a known technique in water treatment, and a relatively common hydraulic application is the aeration cascade[9]. In-stream weirs have been specifically built along eutrophic streams[10]. More generally, in-stream structures may contribute to the aeration and re-oxygenation during overflow operation[9, 11] (Figs. 1(a) and 1(c)). The stepped weir is a very efficient design because of the strong turbulent mixing, the large residence time and the substantial air bubble entrainment[11-12]. Figure 1 presents examples of two instream stepped weirs and a steep stepped spillway. While the structures were not specifically designed for re-aeration, their highly aerated turbulent overflows contribute implicitly to mass and heat exchange, including gas transfer enhancement in the waterways. On the other hand, excessive self-aeration may lead to supersaturation of dissolved nitrogen, with adverse impact on aquatic life, e.g., "gas bubble disease"[8].

While there has been an increasing number of air-water flow measurements in the last two decades, most data sets focused on the void fraction and interfacial velocity. Only a limited number of studies included detailed interfacial data and air-water mass

Biography: Yvan Arosquipa Nina (1992-), Male, Master,
E-mail: yvan.arosquipa@gmail.com
Corresponding author: Hubert Chanson,
E-mail: h.chanson@uq.edu.au

transfer measurements. Notable seminal studies of air-water mass transfer in stepped channels included Toombes and Chanson[11] and Schlenkhoff and Bung[12]. To date, the literature on aeration performances at stepped weirs and cascades has been focused on flat-slope cascades and embankment dam stepped chutes. The current study aims to characterize the interfacial properties and aeration performance of a steep stepped weir. A detailed experimental investigation of air-water flow properties was undertaken with three step configurations, encompassing horizontal and inclined downward steps. The measurements were performed in a relatively large facility with a 45° chute (1V:1H), with a focus on the air-water interfacial flow properties. It is the aim of this study to quantify the aeration potential in terms of dissolved oxygen (DO) of steep stepped weirs.

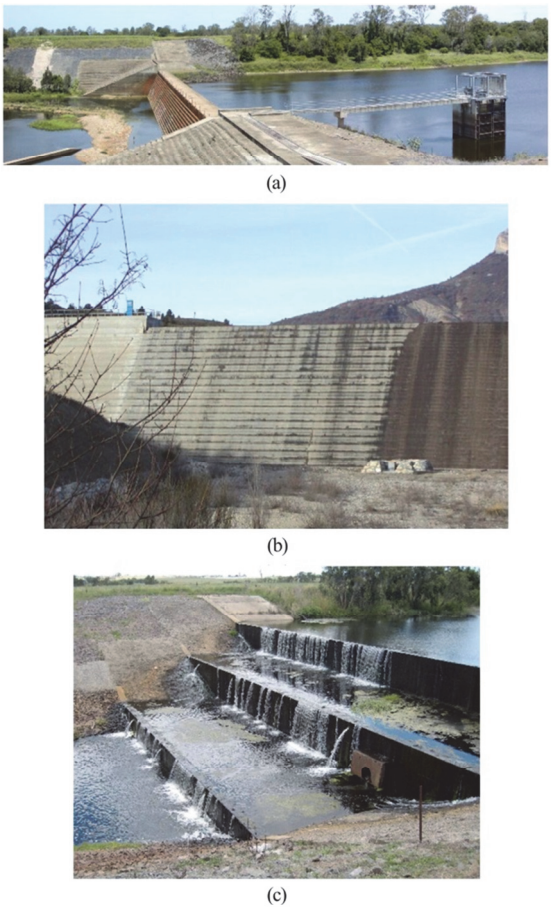

Fig. 1 (Color online) Stepped weirs and cascades. (a) Bucca weir, Bundaberg QLD (Australia) on December 23, 2001– $\theta = 63°$, $h = 0.60$ m , RCC construction, (b) Riou dam, Saint-Genis (France) on February 15, 2004– $\theta = 59°$, $h = 0.43$ m , RCC construction, (c) Joe Sippel Sippel weir, Murgon QLD (Australia) on January 15, 2009 (Courtesy of Damien Roman)-Sheet-pile, concrete construction ($h \sim 2.00$ m)

1. Physical modelling and facility

1.1 *Experimental facility and instrumentation*

The physical experiments were conducted in a 5.0 m long, 1.7 m high and 0.985 m wide test section, in which a 1.2 m high stepped weir was installed. The weir consisted of a 1.2 m high vertical upstream wall, a 0.6 m long broad-crested weir with rounded edges, and a downstream stepped chute with twelve 0.1 m high 0.1 m long steps (Fig. 2). The longitudinal steep chute slope was 45° (1V:1H). The reference configuration consisted of horizontal steps, while two further configurations were equipped with inclined downward steps: 1V:5H (11.3°) and 1V:2.33H (23.2°). Figures 2 and 3 present photographs of the steep stepped chute in operation with different step configurations.

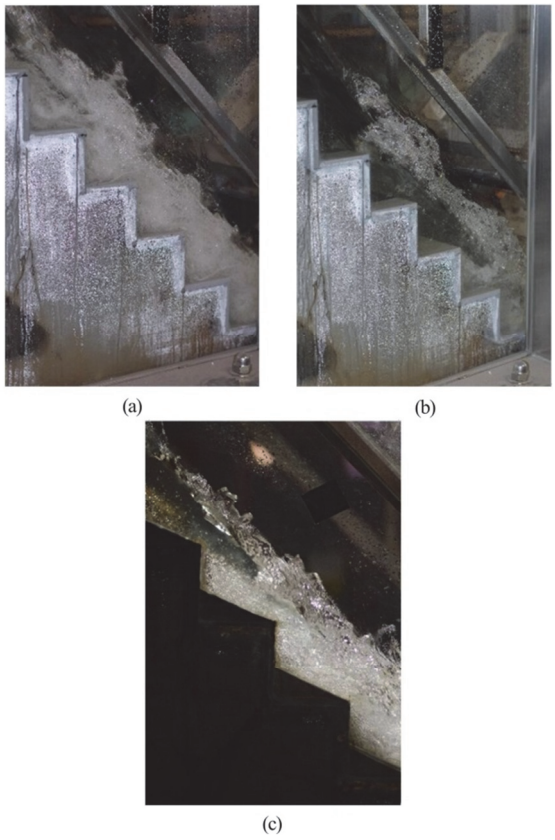

Fig. 2 (Color online) Stepped weir model operation in skimming flow regime– $\theta = 45°$, $h = 0.10$ m , 12 steps. (a) $d_c / h = 1.2$, Horizontal steps (shutter speed: 1/180 s, flash), (b) $d_c / h = 1.6$, Horizontal steps (shutter speed: 1/180 s, flash), (c) $d_c / h = 1.2$, 1V:2.33H inclined steps (shutter speed: 1/5 000 s)

The discharge was measured based upon the head above crest and the rating curve of the broad-crested weir[13]. The void fraction, bubble frequency, inter-

facial velocity and bubbly flow structure were recorded with double-tip conductivity probes. The two tips were identical and equipped with 0.25 mm sensor. The probe signals were scanned for 45 s at 20 kHz per sensor, following sensitivity studies[14-15]. The probes were translated on a trolley system equipped with a fine traverse system, with an accuracy of less than 0.1 mm in the direction normal to the pseudo-invert formed by the outer step edges. The signals were processed following Chanson and Toombes[16] and Felder and Chanson[17]. Additionally, visual observations were made with a dSLR camera and two digital cameras with high-speed movie recording capabilities. Further information was documented in Arosquipa Nina et al.[18].

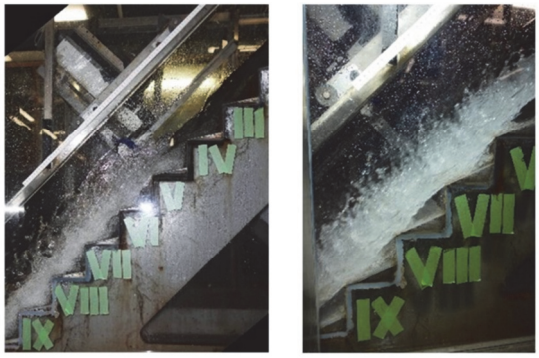

(a) (b)

Fig. 3 (Color online) Stepped weir model operation in transition flow regime– $\theta = 45°$, $h = 0.10$ m, 12 steps. (a) $d_c / h = 0.8$, 1V:5H inclined steps (shutter speed: 1/500 s), (b) $d_c / h = 0.7$, 1V:2.33H inclined steps (shutter speed: 1/500 s)

1.2 *Experimental flow conditions*

The present study focused on the interfacial properties of skimming flows, common in modern steep stepped chutes, although transition flow conditions were observed for the smallest discharge (Table 1). In the skimming flow regime, the water flow is parallel to the pseudo-bottom formed by the step edges, with some strong cavity recirculation in the steps. In the current study, a Froude and Morton similitude was applied and the physical experiments were undertaken in a large size facility with $h = 0.10$ m operating at large Reynolds numbers: i.e., $2.8 \times 10^3 < Re < 1.0 \times 10^6$ [18]. The laboratory conditions may correspond to a 1:4 to 1:6 scale study of the stepped spillway designs shown in Figures 1(a) and 1(b), to ensure the extrapolation of the physical data to prototype conditions with minimum scaling effects.

The air-water flow measurements were undertaken for flow rates between 0.070 m^3/s and 0.198 m^3/s (Table 1). Table 1 summarises the experimental conditions. For each flow rate and each stepped chute configuration, the measurements were performed at all step edges downstream of the inception of free-surface aeration, on the channel centreline. The air-water flow was gradually-varied and uniform equilibrium conditions were not observed down the 12 steps weir for all investigated flow conditions.

2. Basic properties

2.1 *Presentation*

The overflow presented some chaotic motion with strong spray and splashing for the smallest flow rate $d_c / h = 0.7$, 0.8, with d_c the critical flow depth, h

Table 1 Air-water flow measurements on 45° stepped chute with horizontal and inclined steps (present study)

Geometry	Step slope	d_c / h	Re	Inception (step edge)	Flow regime
Geometry I, $\theta = 45°$, $h = 0.10$ m, l –0.10 m	0	0.8	2.8×10^5	3	Transition
		1.0	3.9×10^5	4-5	Skimming
		1.2	5.2×10^5	5	Skimming
		1.4	6.5×10^5	6	Skimming
		1.6	8.0×10^5	6-7	Skimming
Geometry II, $\theta = 45°$, $h = 0.10$ m, l –0.10 m	1V:5H	0.8	2.8×10^5	4	Transition
		1.0	3.9×10^5	4-5	Skimming
		1.2	5.2×10^5	5	Skimming
		1.4	6.5×10^5	6-7	Skimming
		1.6	8.0×10^5	7-8	Skimming
Geometry III, $\theta = 45°$, $h = 0.10$ m, l –0.10 m	1V:2.33H	0.8	2.8×10^5	4	Transition/ skimming
		1.0	3.9×10^5	5-6	Skimming
		1.2	5.2×10^5	8	Skimming
		1.4	6.5×10^5	7-8	Skimming
		1.6	8.0×10^5	10	Skimming

Notes: d_c: Critical flow depth, h: Vertical step height measured from step edge to step edge; l: Horizontal step length, Re: Reynolds number defined in terms of the hydraulic diameter D_H, e.g., for a wide channel $Re = \rho 4q / \mu$, θ: Slope between pseudo-bottom formed by step edges and horizontal, Inception: Location of inception of free-surface aeration.

the vertical step height. This is illustrated in Fig. 3. The overflow was strongly aerated along the entire chute. The air-water mainstream flowed overall parallel to the pseudo-invert formed by the outer step edges despite the existence of some air cavities existed beneath the nappes. Such air cavities are seen in Fig. 3, with their shapes changing from step to step.

For larger discharges ($d_c / h \geq 1$), the water skimmed over the outer step edges, with intense cavity recirculation in the stepped cavities (Fig. 2). Figure 2 presents some typical sideview photographs of skimming flows. The location of the inception of free-surface aeration shifted downstream with increasing flow rate. This is illustrated by comparing Figs. 2(a) and 2(b), taken from the same perspective (with same shutter speed) for two different flow rates, i.e., $d_c / h = 1.2$ and 1.6 respectively. The introduction of inclined downward steps yielded a smaller cavity volume, as seen in Fig. 2(c). While the cavity was triangular and symmetrical with horizontal steps, the step cavity shape became more elongated and asymmetrical with inclined steps. Visual observations using high-speed movies suggested that the recirculation motion was more unstable.

2.2 *Void fraction and interfacial velocity distributions*

Downstream of the inception region, strong self-aeration took place and the free-surface was visually white. The air entrainment was characterised by the distributions of void fraction, defined as the volume of air per unit volume of air and water, recorded at step edges. Typical results are presented in Fig. 4, where y is the distance normal to the pseudo-invert formed by the step edges, Y_{90} is the characteristic distance where $C = 0.90$, x is the longitudinal distance down the downstream end of the broad-crested weir and λ is the step cavity length, i.e., $\lambda = (h^2 + l^2)^{1/2}$ with $h = l = 0.10$ m in the current study. At a given step edge, the void fraction increased from small values next to the stepped invert to unity above the overflow. The data followed closely theoretical solutions of the advective diffusion of air in the self-aerated flows[16].

Overall, the void fraction data showed a substantial air entrainment on the steep stepped chute, with little difference between the three step configurations. This is illustrated in Fig. 5 showing typical longitudinal distributions of depth-averaged void fraction C_{mean} for two discharges. The data showed a very rapid aeration of the flow immediately downstream of the inception region, while the mean air content tended to some value about 0.35-0.40 at the downstream end of the weir chute for all investigated conditions (Fig. 5).

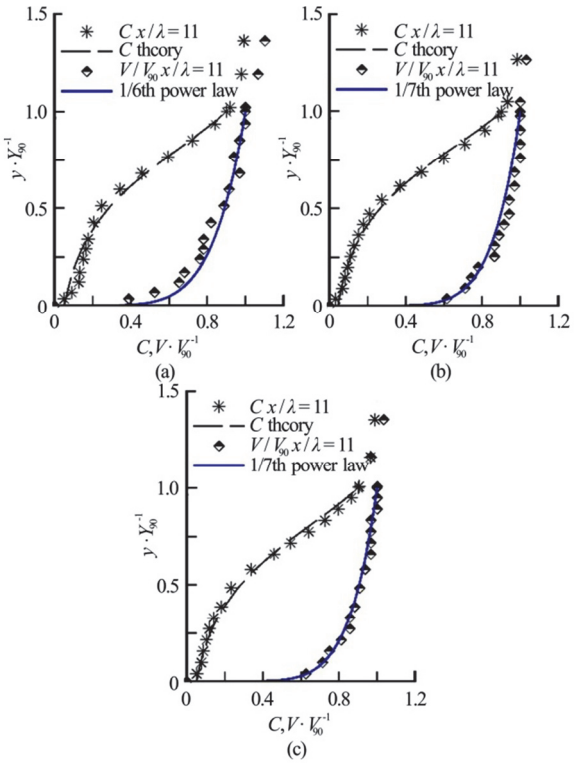

Fig. 4 (Color online) Dimensionless distributions of void fraction C, interfacial velocity V / V_{90} at the downstream end of a steep stepped weir– $\theta = 45°$, $h = 0.10$ m, 12 steps, $d_c / h = 1.0$, last step edge. (a) Horizontal steps, (b) 1V:5H inclined steps, (c) 1V:2.33H inclined steps

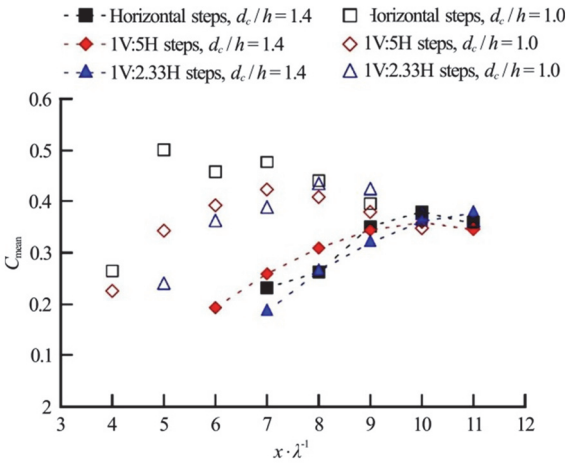

Fig. 5 (Color online) Dimensionless longitudinal distributions of depth-averaged void fraction C_{mean} on a steep stepped weir– $\theta = 45°$, $h = 0.10$ m, 12 steps, $d_c / h = 1.0, 1.4$

The velocity data, obtained through a cross-correlation of the signals recorded at the leading and

trailing tips, showed an accelerating flow down the steep stepped chute. At each step edge, the distributions of velocity tended to follow a power law for $0 < y < Y_{90}$, as seen in Fig. 4. Above, i.e., $y > Y_{90}$, the velocity profile tended to be more uniform.

3. Air-water flow structure

3.1 *Bubble frequency*

For a given void fraction, the number of detected interfaces gave a quantitative description of the fragmentation of the air-water flow. Herein the bubble frequency is defined as half the number of air-to-water and water-to-air interface detections per unit time. Typical profiles are presented in Fig. 6(a). All the profiles indicated a maximum bubble frequency about the mid-air-water column, while showing slightly large bubble frequencies on the inclined step chute. Along the steep stepped chute, the maximum value increased with longitudinal distance (Fig. 6). Typical longitudinal distributions of maximum bubble frequency are presented in Fig. 6(b). The finding was similar to earlier results on stepped chutes across a wide range of chute slopes[18-20].

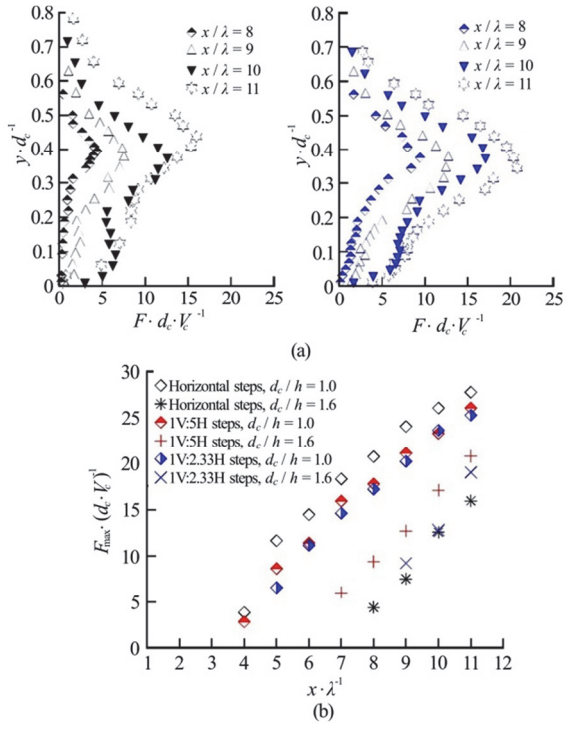

Fig. 6 (Color online) Dimensional distributions of bubble frequency on steep stepped weir– $\theta = 45°$, $h = 0.10$ m, 12 steps. (a) Vertical profiles of bubble frequency Fd_c / V_c for $d_c / h = 1.6$ for horizontal steps (Left), 1V:5H inclined steps (Right), (b) Dimensional longitudinal distributions of maximum bubble frequency $F_{max} d_c / V_c$

For all the observations, the relationship between bubble frequency and void fraction showed a quasi-parabolic trend (Fig. 7). The present data were systematically compared to a theoretical model[21]

$$\frac{F}{F_{max}} = \frac{1}{\alpha_F \beta_F} \frac{C(1-C)}{C_{F_{max}}{}^2} \tag{1}$$

where F_{max} is the maximum bubble rate at a cross-section, α_F and β_F are two correction factors functions of the local void fraction C and flow conditions, and $C_{F_{max}}$ is the void fraction for which $F = F_{max}$. α_F accounts for the different average sizes of air bubble chord size λ_a and water droplet chord size λ_w

$$\alpha_F = 1 + \left(\frac{\lambda_w}{\lambda_a} - 1 \right) C \tag{2}$$

with the ratio λ_w / λ_a assumed to be constant within a cross-section independently of the void fraction[21]. β_F takes into account the variation of λ_w and λ_a with the void fraction

$$\beta_F = 1 - b(1-2C)^4 \tag{3}$$

where b is a characteristic value of the maximum variation of β: i.e., $1 - b < \beta_F < 1$. Both α_F and β_F are theoretically related to the local void fraction $C_{F_{max}}$ where $F = F_{max}$.

$$\alpha_F \beta_F = \frac{1 - C_{F_{max}}}{C_{F_{max}}} \tag{4}$$

For all experiments, Eq. (1) fitted well the experimental data and some typical distributions are shown in Fig. 7. For the present data set, the values of λ_w / λ_a and b were within $0.65 < \lambda_w / \lambda_a < -3.60$ and $0.25 < b < 0.78$ (Table 2). Table 2 summarises the present observations and shows a comparison with past studies.

The quasi-parabolic relationship between bubble frequency and void fraction across the air-water column implied a monotonic relationship between bubble frequency and interfacial turbulence intensity[22]. For all investigated flow conditions (Table 1), the relationship between bubble frequency and void fraction exhibited an increased skewness with increasing downstream distance from the inception point.

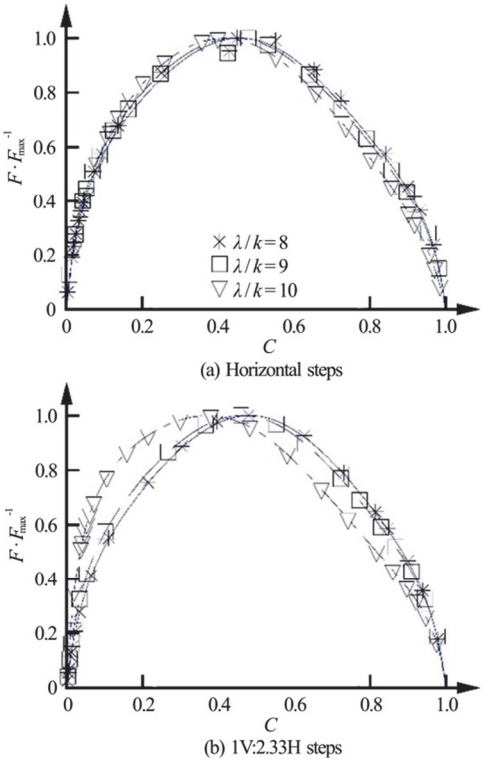

Fig. 7 (Color online) Dimensionless relationship between bubble frequency F / F_{max}, void fraction C on steep stepped weir– $\theta = 45°$, $h = 0.10$ m, 12 steps, $d_c / h = 1.4$ –Comparison with Eq. (1) (Blue lines)–Legend provides detailed conditions

3.2 *Bubble/drop sizes and clustering*

The bubble and water drop chords were extracted from the double-tip probe signals. Herein, bubble chords were analysed in the bubbly flow region only, defined as $C < 0.3$, while water drop chords were only investigated in the spray region, i.e., $C > 0.7$. Typical quantitative data are presented in Fig. 8, as histograms of bubble/drop chords at the last step of the steep chute. In Fig. 8, each column gives the probability of bubble/drop chords in 0.5 mm intervals. For all investigations, the probability of bubble chords was the largest for particle sizes between 0.5 mm and 2.0 mm (Fig. 8(a)), while the water drop chord probability was the largest for droplet sizes between 1 mm and 4 mm (Fig. 8(b)). The histograms were skewed, although a greater skewness was observed with bubble chords compared to drop chords, for a comparable void/liquid fraction. This is seen in Fig. 8, in which the data are shown with similar void/liquid fractions. Overall, the bubble/drop chord results were comparable to previous studies on flatter stepped chutes[16, 19, 23]. Further, the histograms of bubble/drop chords were close for all the three step geometries, in the current study.

The entrained bubbles/droplets interacted with the air-water flow turbulent structures, yielding some turbulent dissipation and the formation of bubble clusters[24-25]. Visual observations highlighted some strong preferential bubble accumulation, i.e. clustering, in the air-water cavity region and in the shear layer downstream of step edge. Herein the cluster analyses were based upon the near-wake criterion[26]. That is,

Table 2 Dimensionless relationship between bubble frequency F / F_{max}, void fraction C: Observed values of the dimensionless coefficients λ_w / λ_a, b (Eqs. (1)-(3))

References	Configuration	λ / k	λ_w / λ_a	b
Present study	$\theta = 45°$, $h = 0.10$ m, $B = 0.985$ m	-	-	-
	Horizontal steps	2.0	1.00-2.70	0.25-0.78
	1V:5H steps	2.5	0.75-3.10	0.30-0.75
	1V:2.33H steps	3.0	1.10-3.60	0.65-0.75
Toombes[36]	$\theta = 2.6°$, $h = 0.143$ m, $B = 0.25$ m	22.1	-	-
	Lower nappe	-	1.25	0.40
	Upper nappe	-	1.00	0.40
	Nappe impact	-	1.75	0.60
	Downstream flow	-	0.55-1.25	0.40
Gonzalez[23]	$\theta = 15.9°$, $h = 0.10$ m, $B = 1.0$ m	3.8	1.75	0.41-0.71
	$\theta = 21.8°$, $h = 0.10$ m, $B = 1.0$ m	2.9	1.75	0.40-0.68
Felder[15]	$\theta = 26.6°$, $h = 0.10$ m, $B = 1.0$ m	2.5	1.0-2.40	0.40-0.60

Notes: B: Channel width; h: vertical step height measured from step edge and step edge, k: step cavity depth measured normal to the pseudo-bottom formed by the step edges, λ: Step cavity length measured along the pseudo-bottom formed by the step edges.

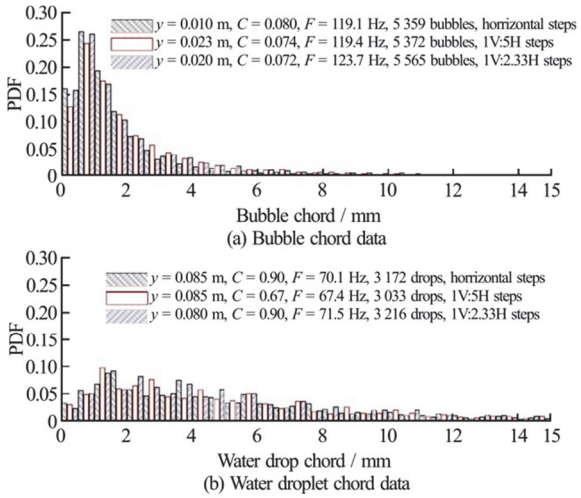

Fig. 8 (Color online) Normalised probability distribution functions of bubble/droplet at the downstream end of a steep stepped weir– $\theta = 45°$, $h = 0.10$ m, 12 steps, $d_c / h = 1.4$, last step, chord histograms with 0.5 mm intervals–Legend gives local air-water flow properties including void fraction C, bubble frequency F. (a) Bubble chord data, (b) Water droplet chord data

the identification of a bubble cluster was undertaken based upon the analysis of the water chord between two successive air bubbles and a cluster was detected when the trailing particle was in the near-wake of the lead one: i.e., the trailing particle was at a distance less than the air chord of the leading bubble. The method was applied to the bubbly flow region $(C < 0.3)$ and spray region $(C > 0.7)$ only.

For all flow conditions and step geometries, the results indicated a relatively large proportion of particles (bubbles/droplets) travelling within some cluster structure. As the void/liquid fraction increased, the probability of finding neighbouring particles at closer distances increased, and the percentage of particles in clusters, as well as the average number of particles per cluster, increased as shown in Fig. 9. Figure 9(a) presents the percentage of particles in a cluster. A relatively large proportion of particles travelled as part of a cluster, with the percentage of particles in cluster ranging from 15% to 60% depending upon the void fraction (Fig. 9(a)). The data set includes both bubbly flow $(C < 0.3)$ and spray $(C > 0.7)$ regions. Figure 9(b) shows the average number of particles per cluster in both lower bubbly flow and upper spray regions. An absolute majority of particle clusters consisted of two particles only (Fig. 9(b)). For completeness, Fig. 10 illustrates some typical probability distribution func- tions of number of bubbles per cluster for a similar void fraction.

Finally, the present cluster results were based upon an one-dimensional analysis, ignoring two- and three-dimensional particle clusters. Recent studies suggested that, in free-surface air-water flows, the number of bubbles/drops in two-dimensional clusters was in average at least 15%-20% larger than the corresponding number of streamwise clustered bubbles[27].

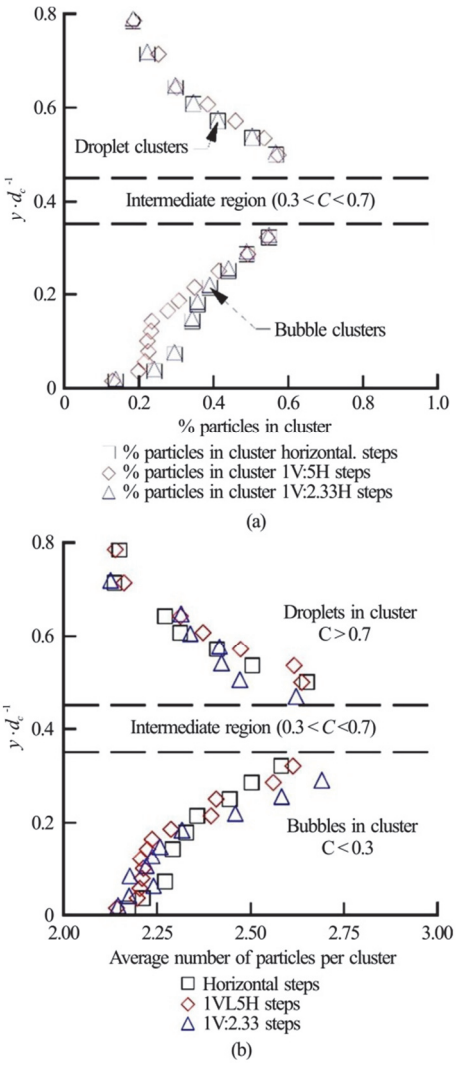

Fig. 9 (Color online) Clustering properties at the downstream end of a steep stepped weir– $\theta = 45°$, $h = 0.10$ m, 12 steps, $d_c / h = 1.4$, last step–Legend provides configuration details. (a) Dimensionless distributions of percentage of bubbles $(C < 0.3)$ and drops $(C > 0.7)$ in clusters, (b) Dimensionless distributions of average number of particles in cluster

4. Interfacial properties and aeration

4.1 *Interfacial area*

At a hydraulic structure, the gas transfer process is driven by Fick's law, i.e., the mass transfer rate

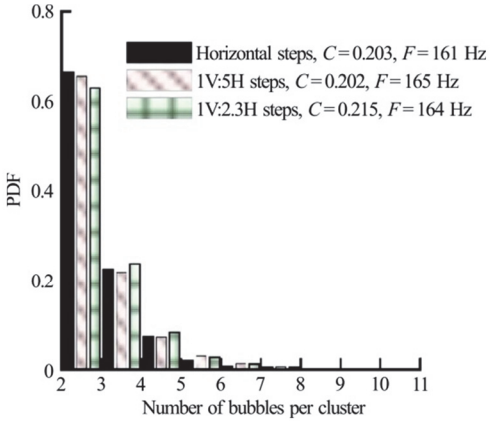

Fig. 10 (Color online) Probability distribution functions of the number of bubbles per cluster at the downstream end of a steep stepped weir– $\theta = 45°$, $h = 0.10$ m, 12 steps, $d_c / h = 1.4$, last step–Legend provides air-water flow details

across an interface varies proportionally to a diffusion coefficient times the gradient of gas concentration. For a volatile gas (e.g., oxygen), the transfer is controlled by the liquid phase and the basic equation for gas transfer across the air-water interface may be expressed as (Appendix A):

$$\frac{\partial C_{gas}}{\partial t} = K_L \frac{a}{1-C}(C_{SAT} - C_{gas}) \tag{5}$$

where K_L is the mass transfer coefficient or liquid film coefficient, a is the specific interface area defined as the interface area per unit volume, C is the void fraction with $1-C$ representing the liquid fraction, C_{gas} is the dissolved gas concentration and C_{SAT} is the amount of gas dissolved in water at equilibrium. Equation (5) shows that the rate of mass transfer is directly proportional to the air-water interface area and to the transit time. Thus, it is highly enhanced in self-aerated turbulent flows down stepped chutes[11].

In self-aerated flows, the specific interface area a is the cumulative surface of all air bubbles and water droplets per unit volume of air and water, and it may be estimated as[28]

$$a = \frac{4F}{V} \tag{6}$$

The specific interface area distributions were calculated for all unit discharges within $0.07\ m^2/s < q < 0.20\ m^2/s$ at all step edges downstream of the inception point of free-surface aeration. At a step edge, the depth-averaged specific interface area a_{mean} was calculated as

$$a_{mean} = \frac{1}{Y_{90}} \int_0^{Y_{90}} a dy \tag{7}$$

Typical specific interface area data are presented in Fig. 11, in a dimensional form to emphasise the magnitude of interfacial areas in the self-aerated flows. Typical vertical distributions are shown in Fig. 11(a). All the profiles presented a marked maximum at the location of maximum bubble frequency. Some typical longitudinal distributions of depth-averaged specific interface area are presented in Figs. 11(b) and 11(c). The mean specific interface area increased monotonically with increasing distance downstream of the inception point, as the chute flow became more aerated and fragmented.

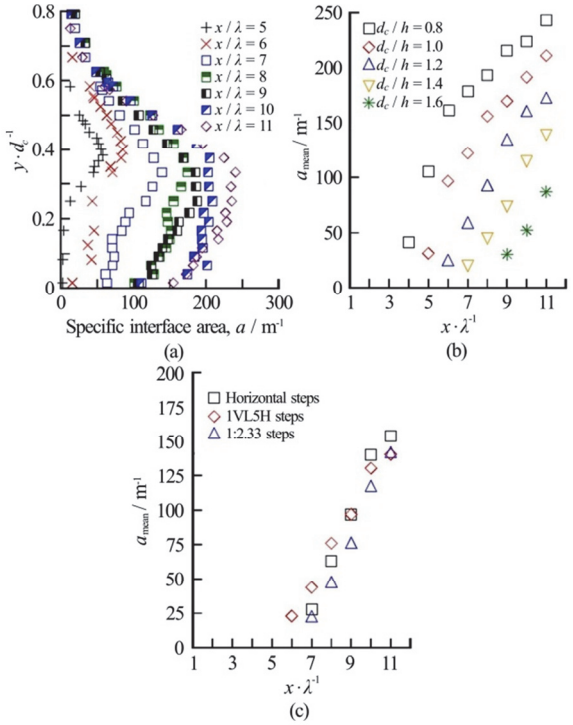

Fig. 11 (Color online) Specific interface area in self-aerated flows on a steep stepped weir– $\theta = 45°$, $h = 0.10$ m, 12 steps–Legend provides detailed conditions. (a) Vertical distributions of specific interface area– $d_c / h = 1.2$, $Re = 5.2 \times 10^5$, 1V:5H stepped chute, (b) Longitudinal distributions of depth-averaged specific interface area on 1V:2.33H stepped chute. (c) Longitudinal distributions of depth-averaged specific interface area for $d_c / h = 1.4$, $Re = 8.5 \times 10^5$ –Comparison between the three stepped geometries

The largest specific interfacial areas were recorded in the transition flow regime, with depth-

averaged specific areas up to 300 m^2 per unit volume, corresponding to dimensionless specific area $a_{mean} d_c$ up to 25. In skimming flows, the interfacial area data decreased with increasing flow rate, as the inception of free-surface aeration shifted further downstream. For a given discharge, the interface area levels were generally smaller, by about 10%, on the inclined downward stepped chutes than on the horizontal stepped weir, in average for all tested flow conditions. Despite the larger bubble frequencies (Fig. 6(a)), the specific interfaces for the inclined configurations were smaller than on the horizontal steps because to the larger velocities.

4.2 *Aeration efficiency*

Considering the steep chute, the rate of mass transfer may be derived from the integration of Fick's law (Eq. (5))

$$\frac{\partial C_{gas}}{\partial x} = \frac{K_L a_{mean}}{V_{mean}(1-C_{mean})}(C_{SAT} - C_{gas}) \quad (8)$$

where C_{mean} is the depth-averaged void fraction and V_{mean} is the mean flow velocity: $V_{mean} = q/d$ with q the unit discharge and d the equivalent clear-water depth

$$d = \int_0^{Y_{90}} (1-C)dy = (1-C_{mean})Y_{90} \quad (9)$$

The coefficient of mass transfer K_L was estimated as $K_L = 4.40 \times 10^{-4}$ m/s for oxygen at $T = 20°C$ (Appendix B). Such a value is comparable to measured liquid film coefficients in turbulent streams[29-30], in stepped cascades[11].

The complete integration (Eq. (8)) was performed for all dimensionless discharges $0.8 < d_c/h < 1.6$ $(2.8 \times 10^5 < Re < 8.0 \times 10^5)$ and configurations based upon the measured air-water flow properties. The results are presented in Fig. 12 in terms of the aeration efficiency E at 20°C of the stepped weir for dissolved oxygen, with E being defined as

$$E = \frac{C_{DS} - C_{US}}{C_{SAT} - C_{US}} \quad (10)$$

where C_{US} and C_{DS} are respectively the upstream and downstream dissolved oxygen concentrations. The present data showed that the aeration efficiency decreased with increasing discharges, for all configurations (Fig. 12). This was linked to the further downstream location of inception region, the lesser aeration of the chute and the associated reduction in interfacial area with increasing flow rate (Fig. 11(b)). The horizontal step chute experienced the greatest aeration efficiency, while the smallest aeration was observed with the 1V:2.33H inclined downward steps.

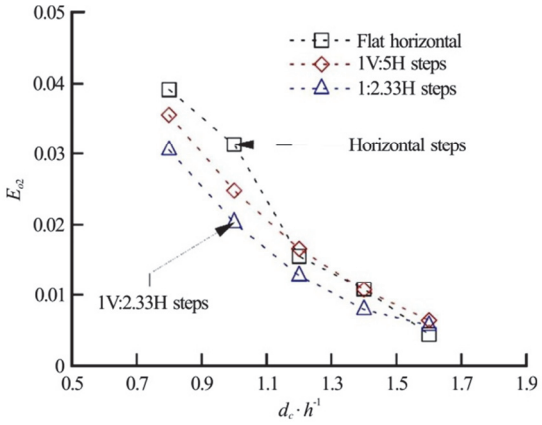

Fig. 12 (Color online) Dissolved oxygen aeration efficiency of a steep stepped weir– $\theta = 45°$, $h = 0.10$ m, 12 steps, in terms of dissolved oxygen at 20 Celsius– Legend provides stepped geometry

Table 3 Dissolved oxygen aeration efficiency experiments on stepped chutes with detailed air-water flow measurements and dissolved oxygen measurements

θ /°	h /m	λ / k	Geometry	$\Delta z_0 / h$	Flow regime	Refenences
45	0.10	2.0 2.5 3.0	Horizontal steps 1V:5H steps 1V:2.33H steps	11	Skimming and Transation	Present[2, a]
45	0.05	2.0	Horizontal steps	40	Skimming	Ref. [37][1]
26.6	0.06	2.5	Horizontal steps	39	Skimming	Ref. [12][1, b]
21.8	0.05	2.9	Horizontal steps	30, 40	Skimming	Ref. [37][1]
15	0.50	4.0	Horizontal steps	6	Nappe	Ref. [38][1]
3.4	0.143	16.9	Horizontal steps	12	Transation and Skimming	Ref. [11][1, 2, c]

Notes: [1]: Detailed dissolved oxygen (DO) measurements, [2]: Air-water flow data obtained from the integration of the mass transfer equation (Eq. (8)), [a]: Probe sensor size: 0.25 mm, [b]: Probe sensor size: 0.13 mm, [c]: probe sensor size: 0.025 mm.

The current data compared reasonably well to some dissolved oxygen measurements on stepped chute laboratory facilities (Table 3). Table 3 presents the key features of these studies. Figure 13 shows the aeration efficiency per metre drop in invert elevation, i.e., $E / \Delta z_0$, in terms of dissolved oxygen at 20 Celsius, standard pressure and zero salinity as a function of the measured rate of energy dissipation $\Delta H / H_{max}$. Herein, $\Delta H / H_{max}$ was estimated based upon the air-water flow measurements and the data are reported in Table 1. In skimming flows, the data showed a monotonic increase in re-aeration per unit height with increasing rate of energy dissipation, that was linked to the longer aeration region in presence of long chutes with large transit times. Combining the present data with dissolved oxygen data sets, the relationship between aeration efficiency per metre drop in invert elevation and rate of energy dissipation was best correlated as

$$\frac{E}{\Delta z_0} = 0.5075 \times \left(\frac{\Delta H}{H_{max}} \right)^{4.4} \quad (11)$$

where Δz_0 is the drop in elevation, ΔH is the head loss and H_{max} is the upstream total head. Equation (11) is compared to the experimental data in Fig. 13.

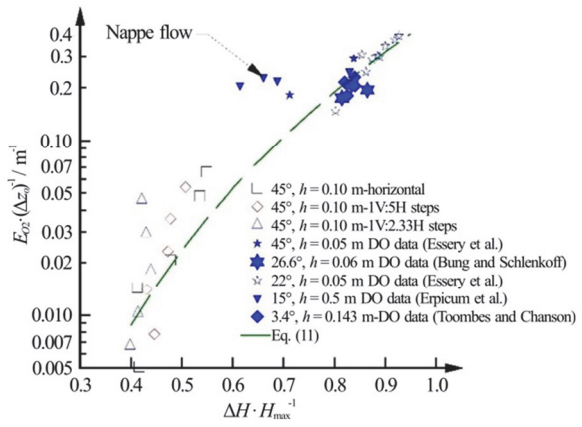

Fig. 13 (Color online) Aeration efficiency per metre drop in invert elevation $E / \Delta z_0$ in terms of dissolved oxygen at 20 Celsius in skimming flows on stepped chutes, calculated based upon detailed air-water flow measurements–Comparison between air-water flow data obtained from the integration of the mass transfer equation (Eq. (8)), dissolved oxygen measurements (Table 3), Eq. (11) (thin dashed line)

In summary, the integration of the Fick's law allowed a comparison of aeration performances between horizontal and inclined downward stepped chute. Both the specific interface areas and aeration efficiency were smaller on the inclined downward stepped chutes, for identical discharges. In other words, the flat horizontal step configuration provided a better re-oxygenation rate than inclined step weirs. A comparison with previous data showed a good agreement for stepped channels with slopes within $3.4° < \theta < 45°$, highlighting a monotonic increase in re-aeration with increasing rate of energy dissipation.

5. Conclusions

The aeration performance of a steep weir with 12 steps was studied based upon a detailed investigation of air-water flow properties. The measurements were performed with a focus on the interfacial flow properties in a relatively large facility with a 45° chute (1V:1H) operating at relatively large unit discharges $(0.07 \text{ m}^2/\text{s} < q < 0.20 \text{ m}^2/\text{s})$. Three step configurations were tested systematically, encompassing horizontal steps and two inclined downward steps.

In terms of basic air-water flow properties, the distributions of void fraction and bubble frequency presented very close results for all three step geometries, both qualitatively and quantitatively. For all flow conditions and step geometries, the histograms of particle chords were skewed, close to a log-normal distribution. The particle clustering analyses showed a relatively large proportion of particles (bubbles/droplets) within some cluster structure. As the void/liquid fraction increased, the probability of finding neighbouring particles at closer distances increased, and the percentage of particles in clusters and average number of particles per cluster, increased. Altogether, the present results suggested that the bubble dynamics within the flow, i.e., number of bubbles, bubble size and bubble/droplet clusters, were little affected by the geometry of the cavity. In contrast, the specific interface area magnitudes were in average smaller, by about 10%, on the inclined downward step chutes compared to the horizontal stepped weir, for a given discharge. The oxygen aeration efficiency was estimated based upon the measured air-water flow properties including interfacial areas. A comparison of present and previous stepped chute data indicated a monotonic increase in re-aeration with increasing rate of energy dissipation for chute slopes within $3.4° < \theta < 45°$. For $\theta = 45°$, the present results showed the largest aeration efficiency being observed on the horizontal step weir chute, and the smallest dissolved oxygen aeration on the 1V:2.33H inclined downward steps.

In summary, a steep stepped chute can make a sizeable contribution to the re-oxygenation of the waters. While the differences at the millimetric and macro-scales were relatively small, the performances of steep stepped weir were impacted by a downward

step slope by a downward step slope. The largest (oxygen transfer) aeration efficiency was observed for flat horizontal steps, while the inclined downward stepped weir chutes being less efficient in terms of DO aeration efficiency.

Acknowledgements

The authors would like to thank Prof. Jorge Matos (IST Lisbon, Portugal), Dr. Brian Crookston (Utah State University, USA) and Prof. Daniel Bung (FH Aachen University of Applied Sciences, Germany), for their detailed comments and helpful suggestions. The authors acknowledge the technical assistance of Jason van der Gevel, Stewart Matthews (The University of Queensland). This work was supported by the Swiss National Science Foundation (Grant No. P2ELP2_181794), the School of Civil Engineering, University of Queensland.

References

[1] Rao N. S. L., Kobus H. E. Characteristics of self-aerated free-surface flows (Water and waste water/current research and practice) [M]. Berlin, Germany: Eric Schmidt Verlag, 1974, 10: 224.

[2] Falvey H. T. Air-water flow in hydraulic structures (USBR Engineering Monograph) [R]. Denver, USA: United States Department of the Interior, Water and Power Resources Service, 1980.

[3] Jevdjevich V., Levin L. Entrainment of air in flowing water and technical problems connected with it [C]. *Proceedings of the 5th International Association for Hydro-Environment Engineering and Research (IAHR)*, Minneapolis, USA, 1953, 439-454.

[4] Chanson H. Drag reduction in open channel flow by aeration and suspended load [J]. *Journal of Hydraulic Research*, 32(1): 87-101.

[5] Wood I. R. Air entrainment in free-surface flows. IAHR Hydraulic Structures Design Manual No. 4 [M]. Rotterdam, The Netherlands: A. A. Balkema, 1991, 149.

[6] Gulliver J. S. Introduction to air-water mass transfer [C]. *Proceedings of the 2nd International Symposium on Gas Transfer at Water Surfaces*, Minneapolis, USA, 1-7.

[7] Chanson H. Air Bubble Entrainment in free-surface turbulent shear flows [M]. London, UK: Academic Press, 401.

[8] Weber L. J., Mannheim C. Unique approach for physical model studies of nitrogen gas supersaturation [C]. *Proceedings of the 27th International Association for Hydro-Environment Engineering and Research (IAHR) Biennial Congress*, San Francisco, USA, 1997, 518-523.

[9] Nakasone H. Study of aeration at weirs and cascades [J]. *Journal of Environmental Engineering*, 1987, 113(1): 64-81.

[10] Gosse P., Gregoire A. Artificial re-oxygenation of the sinnamary, downstream of petit-saut dam (French Guyana) [J]. *Hydroécology Application*, 1997, 9(1-2): 23-56(in French).

[11] Toombes L., Chanson H. Air-water mass transfer on a stepped waterway [J]. *Journal of Environmental Engineering*, 2005, 131(10): 1377-1386.

[12] Schlenkhoff A., Bung D. B. Prediction of oxygen transfer in self-aerated skimming flow on embankment stepped spillways [C]. *Proceedings of the 33th International Association for Hydro-Environment Engineering and Research (IAHR) World Congress*, Vancouver, Canada, 2009.

[13] Zhang G., Chanson H. Hydraulics of the developing flow region of stepped spillways. I: Physical modeling and boundary layer development [J]. *Journal of Hydraulic Engineering, ASCE*, 2016, 142(7): 1-9.

[14] Chanson H. Dynamic similarity and scale effects affecting air bubble entrainment in hydraulic jumps [C]. *Proceedings of the 6th International Conference on Multiphase Flow (ICMF)*, Leipzig, Germany, 2007.

[15] Felder S. Air-water flow properties on stepped spillways for embankment dams: Aeration, energy dissipation and turbulence on uniform, non-uniform and pooled stepped chutes [J]. Doctoral Thesis, Brisbane, Australia: The University of Queensland, 2013.

[16] Chanson H., Toombes L. Air-water flows down stepped chutes: Turbulence and flow structure observations [J]. *International Journal of Multiphase Flow*, 2002, 28(11): 1737-1761.

[17] Felder S., Chanson H. Energy dissipation, flow resistance and gas-liquid interfacial area in skimming flows on moderate-slope stepped spillways [J]. *Environmental Fluid Mechanics*, 2009, 9(4): 427-441.

[18] Arosquipa Nina Y., Shi R. et al. Intrusive and non-intrusive air-water measurements on stepped spillways with inclined steps: A physical study on air entrainment and energy dissipation [R]. Hydraulic Model Report No. CH121/21, Brisbane, Australia: The University of Queensland, 2021.

[19] Chanson H., Toombes L. Experimental study of gas-liquid interfacial properties in a stepped cascade flow [J]. *Environmental Fluid Mechanics*, 2002, 2(3): 241-263.

[20] Yasuda Y., Chanson H. Micro- and macro-scopic study of two-phase flow on a stepped chute [C]. *Proceedings of the 30th International Association for Hydro-Environment Engineering and Research (IAHR) Biennial Congress*, Thessaloniki, Greece, 2003, 695-702.

[21] Toombes L., Chanson H. Interfacial aeration and bubble count rate distributions in a supercritical flow past a backward-facing step [J]. *International Journal of Multiphase Flow*, 2008, 34(5): 427-436.

[22] Zhang G., Chanson H. Self-aeration in the rapidly- and gradually-varying flow regions of steep smooth and stepped spillways [J]. *Environmental Fluid Mechanics*, 2017, 17(1): 27-46.

[23] Gonzalez C. A. An experimental study of free-surface aeration on embankment stepped chutes [D]. Doctoral Thesis, Brisbane, Australia: The University of Queensland, 2017.

[24] Calzavarini E., Berg T. H., van der Toschi F. et al. Quantifying microbubble clustering in turbulent flow from single-point measurements [J]. *Physics of Fluids*, 20(4): 040702.

[25] Chanson H. Hydraulics of aerated flows: Qui Pro Quo? [J]. *Journal of Hydraulic Research*, 2013, 51(3): 223-243.

[26] Chanson H., Aoki S., Hoque A. Bubble entrainment and dispersion in plunging jet flows: freshwater versus seawater [J]. *Journal of Coastal Research*, 2006, 22(3): 664-677.

[27] Sun S., Chanson H. Characteristics of clustered particles in skimming flows on a stepped spillway [J]. *Environ-*

mental Fluid Mechanics, 2013, 13(1): 73-87.
[28] Chanson H. Air-Water Flow measurements with intrusive phase-detection probes. can we improve their interpretation? [J]. *Journal of Hydraulic Engineering, ASCE*, 2002, 128(3): 252-255.
[29] Acuna V., Giogi A., Munoz I. et al. Flow extremes and benthic organic matter shape the metabolism of a headwater Mediterranean stream [J]. *Freshwater Biology*, 2004, 49: 960-971.
[30] Tobias C. R., Bohlke J. K., Harvey J. W. et al. A simple technique for continuous measurement of time-variable gas transfer in surface waters [J]. *Limnology and Oceanography: Methods*, 2009, 7: 185-195.
[31] Moog D. B., Jirka G. H. Stream reaeration in nonuniform flow: Macroroughness enhancement [J]. *Journal of Hydraulic Engineering, ASCE*, 1999, 125(1): 11-16.
[32] Kawase Y., Moo-Young M. Correlations for liquid-phase mass transfer coefficients in bubble column reactors with newtonian and non-newtonian fluids [J]. *Canadian Journal of Chemical Engineering*, 1992, 70: 48-54.
[33] Csanady G. T. The role of breaking wavelets in air-sea gas transfer [J]. *Journal of Geophysical Research*, 1990, 95(C1): 749-759.
[34] Katul G., Mammarella I., Gronholm T. et al. A structure function model recovers the many formulations for air-water gas transfer velocity [J]. *Water Resources Research*, 2018, 54: 5905-5920.
[35] Kitaigorodskii S. A. On the fluid dynamical theory of turbulent gas transfer across an air-sea interface in the presence of breaking wind-waves [J]. *Journal of Physical Oceanography*, 1984, 14(5): 960-972.
[36] Toombes L. Experimental study of air-water flow properties on low-gradient stepped cascades [D]. Doctoral Thesis, Brisbane, Australia: The University of Queensland, 2002.
[37] Essery I. T. S., Tebbutt T. H. Y., Rasaratnam S. K. Design of spillways for re-aeration of polluted waters [R]. CIRIA Report No. 72, London, UK: Construction Industry Research and Information Association, 1978.
[38] Erpicum S., Lodomez M., Savatier J. et al. Physical modeling of an aerating stepped spillway [C]. *Proceedings of 6th IAHR International Symposium on Hydraulic Structures*, Portland, OR, USA, 2016, 591-600.
[39] Cussler E. L. Diffusion mass transfer in fluid systems [M]. Second Edition, Cambridge, UK: Cambridge University Press, 1997, 580.

Appendix A-Air-water gas transfer in self-aerated flows

At a hydraulic structure, the gas transfer process is driven by Fick's law, i.e., the mass transfer rate across an interface varies proportionally to a diffusion coefficient times the gradient of gas concentration[39]

$$\frac{\partial M_{\text{gas}}}{\partial t} = -D\frac{\partial C_{\text{gas}}}{\partial x} \tag{A-A1}$$

where D is the diffusion coefficient, C_{gas} is the dissolved gas concentration in the liquid phase. For a volatile gas (e.g., oxygen), the transfer is controlled by the liquid phase and the basic equation for gas transfer across the air-water interface may be simplified into

$$\frac{\partial C_{\text{gas}}}{\partial t} = K_L \frac{a}{(1-C)}(C_{\text{SAT}} - C_{\text{gas}}) \tag{A-A2}$$

where K_L is the mass transfer coefficient or liquid film coefficient, a is the specific interface area defined as the interface area per unit volume of air and water, C is the void fraction, $a/(1-C)$ represents the cumulative interfacial area per unit volume of water, C_{gas} is the dissolved gas concentration and C_{SAT} is the amount of gas dissolved in water at equilibrium. In self-aerated flows, the interfacial area a is the cumulative surface of all air bubbles and water droplets, and the specific interface area may be estimated as[28]

$$a = \frac{4F}{V} \tag{A-A3}$$

where F is the bubble count rate, V is the interfacial velocity. Many observations in self-aerated flow showed that the relationship between bubble frequency and void fraction showed a quasi-parabolic shape[16, 21]

$$F = \omega C(1-C) \tag{A-A4}$$

where ω is a constant. Thus, Eq. (A-2) may be rewritten

$$\frac{\partial C_{\text{gas}}}{\partial t} = \frac{4\omega C}{V} K_L (C_{\text{SAT}} - C_{\text{gas}}) \tag{A-A5}$$

Assuming a primarily one-dimensional convective process, and integrating over the air-water depth Y_{90}, Eq. (A-5) yields

$$\frac{\partial C_{\text{gas}}}{\partial x} = 4\omega \frac{C_{\text{mean}}}{V_{\text{mean}}^{\ 2}} K_L (C_{\text{SAT}} - C_{\text{gas}}) \tag{A-A6}$$

with C_{mean} the depth-averaged void fraction, V_{mean} the mean flow velocity and C_{gas} becoming the depth-averaged gas concentration in the water phase.

Appendix B-On the liquid film coefficient in bubbly turbulent flows

For volatile gases, e.g., oxygen, the mass transfer resistance in bubbly flows is primarily limited to the liquid side of the bubble interface[31]. The interfacial gas flux is equals to the defect gas concentration in the

liquid phase times the liquid film coefficient K_L

$$J = K_L(C_{sat} - C_{gas}) \quad \text{(A-B1)}$$

where C_{gas} is the gas concentration, C_{sat} is the saturation concentration.

For turbulent shear flows in bubbly column, Kawase and Moo-young[32] estimated the coefficient of mass transfer K_L

$$K_L = 0.47\sqrt{D_{gas}}\left(\frac{\mu}{\rho}\right)^{-1/6}\sqrt[3]{g} \quad \text{(A-B2)}$$

with μ is the dynamic viscosity of water, ρ is the density of water, g is the gravity acceleration and D_{gas} is the molecular diffusivity. Equation (A-B2) was developed by bubbles with diameters greater than 0.25 mm, most common in self-aerated air-water flows[16, 19]. For oxygen at $T = 20°C$, the mass transfer coefficient equals: $K_L = 4.37\times10^{-4}$ m/s, almost constant regardless of bubble size and flow turbulence and comparable to measured liquid film coefficients in turbulent streams[29-30].

A number of theories and experiments suggested that the coefficient of mass transfer K_L may be calculated as[33-34]

$$K_L = \Delta\times\left(\frac{\mu/\rho}{D_{gas}}\right)^{-n} V_f \quad \text{(A-B3)}$$

where V_f is a friction velocity in the liquid phase related to the interfacial stress: $V_f = (\tau/\rho)^{1/2}$, is within 0.062 to 0.110, and n ranges from 0.50 to 0.66. In Eq. (A-B3), the term v/D_{gas} is the molecular Schmidt number, with $v = \mu/\rho$. Commonly, the friction velocity is assumed to be equal to the shear velocity: $V_f \approx V_*(\tau_o/\rho)^{1/2}$. Noteworthy, Eq. (A-B3) was found to be realistic in strong wave breaking with bubbly mixture[35].

The liquid film coefficient may be derived indirectly from a few detailed experiments in self-aerated stepped cascades, combining both two-phase flow measurements and dissolved oxygen transfer data[12]. Typical results in terms of the liquid film coefficients are reported in Fig. A-B1, together with Eqs. (A-B2) and (A-B3), the latter being calculated using observed friction velocities down a 45° stepped weir ($h = 0.10$ m). All the data tended to show a same order of magnitude with $K_L \sim 0.4\times10^{-3}$ m/s - 2.0×10^{3} m/s.

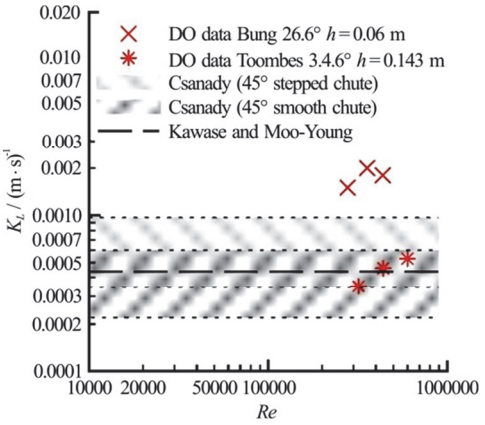

Fig. A-B1 (Color online) Liquid film coefficients in bubbly turbulent flows: comparison between self-aerated stepped cascades[36, 12], Eqs. (A-B2) and (A-B3).